A Multiresolution Method for Tagline Detection and Indexing

Xiaohui Yuan, *Member, IEEE*, Jian Zhang, *Member, IEEE*, and Bill P. Buckles, *Senior Member, IEEE*

***Abstract*—Tagline detection and indexing are challenging tasks due to complicated anatomical properties and imaging noise. In this paper, we will address the following two important issues in tagline detection: 1) an automatic method independent from imaging approaches with improved robustness and accuracy and 2) tagline indexing that matches taglines in task and reference images for postprocessing. Our method consists of two steps: First, a wavelet decomposition is performed on a tagged magnetic resonance (tMR) image. Subband correlation is used to dampen anatomical boundaries but enhance taglines. A tagline map is created by segmenting a reconstructed image using pseudowavelet reconstruction. Next, tagline pixels are grouped into clusters and isolated small line segments are eliminated. A snake method is then used to index and recover broken taglines. Our method has been validated with 320 tMR tongue images. Measurement of tagline accuracy was performed by computing tag pixel displacement. Without assumptions on tagline models, it detects taglines automatically. Comparison studies were conducted against the harmonic phase method. Our experiments resulted in a p-value of 1E–6 with one-way ANOVA, which indicates a significant improvement in accuracy and robustness.**

***Index Terms*—Active contour, image segmentation, magnetic resonance imaging, multiresolution, tagline.**

I. Introduction

TAGGED magnetic resonance (tMR) imaging was developed for *in vivo* studies. It inserts magnetic taglines that essentially create signal voids in tissue using spatially selective presaturation pulses. These taglines appear as dark grids in the image and move with the tissue in motion. It provides a noninvasive means for studying dynamic physiological deformation within tissues. Because the scanned subject can hardly remain still, motion distortions and intrinsic myo-structure interference cause problems in tagline extraction [1].

Several methods were developed for detecting taglines, which attempted to tackle the problem from both the spatial and frequency aspects. Chen and Amini [2] used Markov random fields and maximum *a posteriori* (MAP) estimation, which used manually deployed solid for initial tagline and proceeds to ones with more knots and higher order for smoothness. Deng and Denney [3], [4] described a tagline detection method based on maximum likelihood (ML) and MAP hypothesis testing. It used the image intensity model of a tagline and the initial tagline candidates were estimated across a region-of-interest using a snake algorithm. Several approaches based on snake method [5], [6] were proposed for tagline tracing [7]–[9]. The heuristic applied was the intensity and spatial discontinuity. In [10], Guttman *et al.* proposed a snake-based algorithm and used a high-pass filtered version of the original image. A threshold was used to determine which snake points were parts of a tagline and the spatial continuity constraints were only applied to these points.

Alternatively, frequency-based methods use the tMR imaging property for improved robustness and performance. Osman *et al.* [11], [12] developed a method using harmonic phase (HARP) image. The taglines were reconstructed from band-pass Fourier phase coefficients. Qian *et al.* [13], [14] implemented a tagline segmentation method based on Gabor filter bank. Gabor filters (i.e., Gaussian modulated sinusoid signal) were selected based on prior knowledge such that the first harmonic peak in the frequency domain is extracted. In both methods, filter size has a significant impact on the tagline detection results (a discussion on this is provided in Section II).

Despite the progress made, there is much room for improvement. Thermal noise and image artifacts can cause ambiguities in detecting taglines. The previous methods often rely on empirically chosen coefficients in presumed models. For example, tagline spacing is a factor that needs to be adjusted for images acquired with different tagged imaging protocols. Additional difficulties arise from the subject variation in the task performance. Intrasubject task response variation leads to faded taglines,[1] and the presence of different tissues, fluid, and air degrades taglines. The maximum muscle contraction causes greatly deformed taglines, which could result in tagline-tracing failure.

In this paper, we will address the following two issues in tagline detection.

1) An automatic method that is independent from imaging approaches with improved robustness and accuracy.
2) Tagline indexing that matches taglines in task and reference images for postprocessing.

Our method consists of two steps: First, a wavelet decomposition is performed on a tMR image. Subband correlation is used to dampen anatomical boundaries but enhance taglines. A tagline map is created by segmenting a reconstructed image using pseudo wavelet reconstruction. Next, tagline pixels are grouped into clusters and isolated small line segments are eliminated. A snake method is then used to index and recover broken taglines.

The remainder of this paper is organized as follows: Section II reviews tagged MR image acquisition and its frequency properties. Section III describes our method in two sections: tagline

Manuscript received November 13, 2007; revised March 26, 2008. First published February 2, 2010; current version published March 17, 2010.

X. Yuan and B. P. Buckles are with the Department of Computer Science and Engineering, University of North Texas, Deuton, TX 76207 USA.

J. Zhang is with the Department of Computer Science, Texas Woman's University, Denton, TX 76204 USA.

Color versions of one or more of the figures in this paper are available online at http://ieeexplore.ieee.org.

Digital Object Identifier 10.1109/TITB.2010.2040114

[1]In our studies, tongue press is cued by vocal guidance. Response time of subjects to the vocal cue varies, which causes imaging pulses to mismatch tongue press and results in faded taglines.

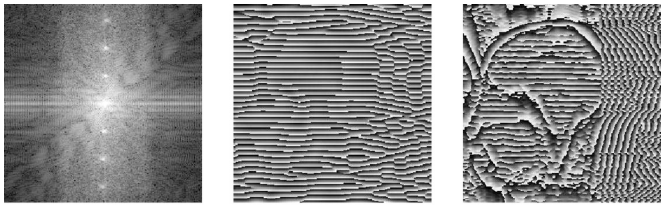

(a) (b) (c)

Fig. 1. (a) k-space image. (b) and (c) Tagline detection with bandpass filter at a size of 9×9 and 41×41, respectively.

segmentation and tagline recovery and indexing. Section IV presents the experiments and analysis using tagged MR images of the tongue. Section V concludes this paper with suggestions for future development.

II. Frequency Characteristics

In tMR imaging, the pulse sequence uses excitation to produce saturated parallel planes throughout the entire imaging volume within a few milliseconds. The image acquisition is performed in a perpendicular plan immediately following the saturation process. A matrix of scanned region, namely k-space image, is then acquired by changing the frequency and phase of the pulse sequence, which essentially consist of Fourier coefficients. The tagline patterns are found to be the spectral peaks in the k-space image, as shown in Fig. 1(a). (Note: the bright spots lined up vertically in the center of the space indicate horizontal taglines.)

Using bandpass filters, taglines can be detected. The choice of the filters, however, is a major factor for accuracy [12]–[14]. Fig. 1(b) and (c) illustrates tagline results produced with the HARP method. Small filters miss the curving taglines [see Fig. 1(b)] due to the lack of frequency components. Large filters invite interference from nearby spectrum peaks. The taglines close to anatomical boundaries are discontinuous [see Fig. 1(c)]. Empirical methods are usually used to select the best bandpass filters.

III. Methodology

A. Tagline Segmentation

The wavelet transform of a function $f(x)$ at scale 2^j, denoted by $W_{2^j} f$, is achieved using convolution with wavelet functions

$$W_{2^j} f(x) \equiv w_j(x) = f(x)\psi_{2^j}(x) \tag{1}$$

where $w_j(x)$ is a wavelet coefficient at x and $\psi(x)$ is a wavelet function. A series of wavelet functions at different scales can be created by dilation using a scale factor 2^j: $\psi_{2^j}(x) = 1/2^j(\psi(x/2^j))$.

The reconstruction of $f(x)$ is achieved via convolution of $w_j(x)$ with a conjugate function $\chi(x)$ as follows:

$$f(x) = \sum_{j=-\infty}^{+\infty} w_j(x)\chi_{2^j}(x). \tag{2}$$

The Fourier transforms of ψ and χ, denoted by $\hat{\psi}$ and $\hat{\chi}$, respectively, satisfy $\sum_{j=-\infty}^{+\infty} \hat{\psi}(2^j\omega)\hat{\chi}(2^j\omega) = 1$.

When applied to an image, the decomposition and reconstruction are performed using discrete scales in an hierarchical filtering scheme. A smoothing function is then used. The wavelets are chosen to be separable products of 1-D functions, applied to images sequentially on rows and columns to generate four subbands at each decomposition scale [15], [16].

The results of a wavelet-transform-resemble edge detection in that each subband consists of gradient values at different scales. Let $\phi(x, y)$ denote a 2-D differentiable smoothing function. The wavelet function ψ consists of a horizontal and a vertical component: $\psi^x(x, y) = \partial\phi(x, y)/\partial x$ and $\psi^y(x, y) = \partial\phi(x, y)/\partial y$. It is shown that the coefficients are the results of the partial derivative of the convolution of image I with filter ϕ. This property has been employed to extract object boundaries with coefficient manipulation and reconstruction [15], [17], [18].

Fig. 2 illustrates the wavelet decomposition of a tMR image with horizontal taglines. Fig. 2(a) shows the low-pass subband (a smoothed image with ϕ) and Fig. 2(b)–(g) shows the gradient subbands. Subbands shown in Fig. 2(b) and (e) depict the tagline features; whereas subbands shown in Fig. 2(c), (d), (f), and (g) contain mostly boundaries of the anatomical structures.

Directional characteristics of wavelet coefficients is the result of applying gradient filters. Hence, a wavelet reconstruction from a set of subbands that contains only the horizontal (or vertical) components enhances the horizontal (or vertical) taglines. In addition, intrascale correlations reveal features that are present across subbands [19], [20]. In our case, such common features encode anatomical boundaries such as cranial outline and spine. By scaling with subband correlation, we can dampen those coefficients that account for the anatomical structure, and hence reduce false tagline detection.

In our algorithm, we use the distance among subbands to describe the subband correlation. The coefficient distance d is computed between two normalized subbands p and q, respectively, in the same decomposition scale

$$d_{p,q}(x, y) = |\tilde{w}_j^p(x, y) - \tilde{w}_j^q(x, y)| \tag{3}$$

where $\tilde{w}_j = |w_j|/\max_i|w_i|$.

Let $\{H, V, D\}$ denote the subband feature direction: horizontal, vertical, and diagonal, respectively, and λ, $\lambda \in \{H, V, D\}$, is the tagline direction. The weights to the tagline subband is computed as follows:

$$\alpha = \frac{d_{A,B} + d_{\lambda,A} + d_{\lambda,B}}{3} \tag{4}$$

where A and B denote the other two subbands with few tagline features. The small values in d imply anatomical boundaries and stationary regions.

Assume we have horizontal taglines, i.e., $\lambda = H$. In the reconstruction, wavelet subbands that contain vertical and diagonal features are replaced with zero matrices. The low-pass subband is substituted with a scaled unity matrix $\mathcal{U}$; whereas the scale is the mean value of the image. The pseudowavelet reconstruction (PWR) is formulated as follows:

$$I' = \mathcal{U} + \sum_{j=1}^{J} (\alpha W_{2^j}^{\lambda} I)\chi_{2^j}. \tag{5}$$

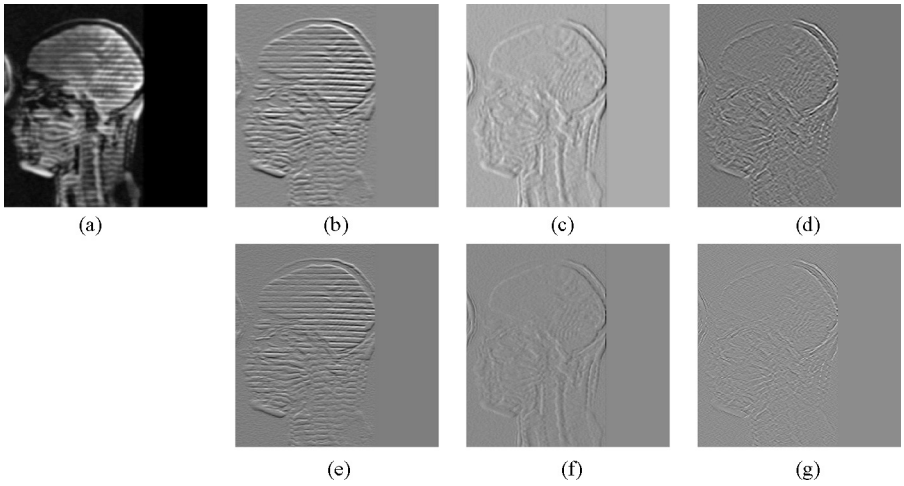

Fig. 2. Wavelet decomposition of a tMR image. (a) Low-pass subband. (b)–(d) Subbands on the second decomposition scale. (e)–(g) Subbands on the first decomposition scale.

Let the tagline map produced by PWR be denoted as I'. We used Otsu's thresholding method [21] to segment taglines. Assume the pixel value in an image is quantized into L bins. The total number of pixels $N = \sum_{i=1}^{L} n_i$ is the sum of the number of pixel n_i in every bin i. Hence, the probability of bin i is computed as $p_i = n_i/N$ and $\sum_{i=1}^{L} p_i = 1$, and $p_i \geq 0$.

Assume a threshold τ is selected to segment taglines. That is, tagline segments consist of pixels with values in the range $[1, 2, \ldots, \tau]$ and the background pixels fall in the range of $[\tau + 1, \tau + 2, \ldots, L]$. The optimal τ is achieved by maximizing the separability criterion

$$\tau = \arg\max_{\tau} \frac{\sigma_B^2}{\sigma_T^2} \tag{6}$$

where σ_B^2 is the between-class variance and σ_T^2 is the image variance

$$\sigma_B^2 = \sum_{i=1}^{\tau} p_i \sum_{j=\tau+1}^{L} p_j \left(\sum_{k=1}^{\tau} \frac{k p_k}{\sum_{m=1}^{\tau} p_m} - \sum_{l=1}^{\tau} \frac{l p_l}{\sum_{n=\tau+1}^{L} p_n} \right)^2 \tag{7}$$

$$\sigma_T^2 = \sum_{i=1}^{L} \left(i - \sum_{j=1}^{L} j p_j \right)^2 p_i. \tag{8}$$

Since the overall variance is functionally independent of τ, an optimal threshold is determined by maximizing the between-class variance

$$\tau = \arg\max_{\tau} \sigma_B^2. \tag{9}$$

B. Tagline Recovery and Indexing

The segmentation results from our previous step give stripe patterns. However, broken taglines and erroneous line segments shall be corrected for tissue motion analysis. For the ease of description, we assume horizontal taglines in the rest of this section.

1) Pixel Clustering and Noise Removal: Let $q(x, y)$ denote a pixel of a tagline in a binary tagline map Q. Assume that tagline pixels in Q have a value of 1. By finding the nearest neighbors and tracing along taglines, we group tagline pixels into clusters. Pixels in a cluster are assigned a new value k. Each pixel in a cluster has at least one neighbor such that the distance is less than a threshold T

$$\begin{aligned} C(k) = &\{q(x, y) = k, \exists q(x', y') \in C(k) \\ &\text{and } \| q(x', y') q(x, y) \| < T\} \end{aligned} \tag{10}$$

where $\| \cdot \|$ denote the Euclidean distance. By counting the number of tagline pixels in every row, we create a projected histogram. An example is shown in Fig. 3. Each peak in the histogram represents a group of connected tagline pixels. Two properties are computed from the projected histogram: cluster distance $\mathcal{D}_{m,n} = |\bar{C}(m) - \bar{C}(n)|$, where $\bar{C}(m)$ and $\bar{C}(n)$ are the means of clusters $C(m)$ and $C(n)$ and cluster size $\mathcal{S}$. With the projected histogram, we first check for broken taglines. Note that because of tagline deformation, peaks in the histogram are mostly skewed and there are overlaps between adjacent peaks.

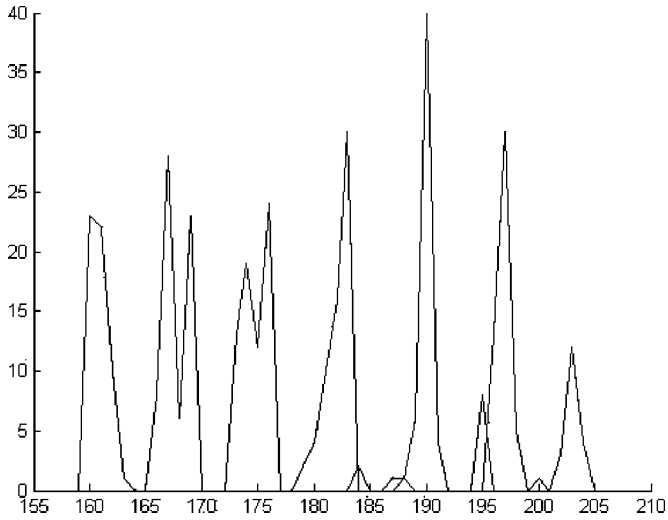

Fig. 3. Projected histogram of tagline.

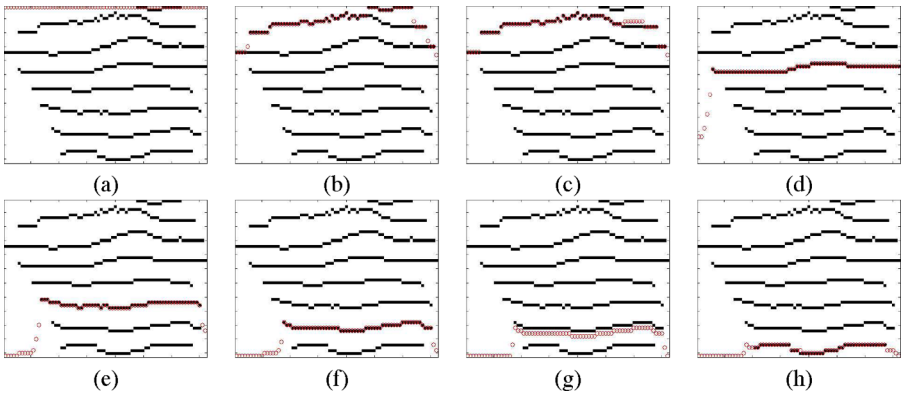

Fig. 4. Evolution of a snake in an experimental run. Taglines are shown in black. The red circles denote the control points on the snake. (a) Initialization of the snake. (b)–(i) Images showing intermediate steps.

Our method examines every pair of clusters $C(n)$ and $C(n-1)$ and combines them if they satisfy the following criteria.

1) The distance of $C(n)$ to an adjacent cluster is less than a threshold $\mathcal{D}^*$, i.e., $\mathcal{D}_{n,n+1} < \mathcal{D}^*$.
2) The distance of $C(n)$ to the closest pixel in one adjacent cluster is less than that in the other adjacent cluster, i.e., $\mathcal{D}_{n,n+1} < \mathcal{D}_{n-1,n}$.

A new label is assigned to the pixels in a combined cluster. This process repeats until no more clusters can be combined. After regrouping, $\mathcal{S}$ is updated. Clusters with small $\mathcal{S}$ are considered as noise and eliminated.

2) Recovery and Indexing: Our tagline recovery and indexing method is derived from the snake model [5], [6], [22]–[24]. However, the snake in our method represents an open contour. Each control point is imposed by elastic forces from neighbors and an external force. The speed is zero at tagline pixels and is one at all other locations. The energy function is an aggregation of external and internal forces as follows:

$$E(s) = E_{\text{ext}} + E_{\text{int}}(s, s-1) + E_{\text{int}}(s, s+1) \tag{11}$$

where E_{ext} is an external force that is enforced equally everywhere in the image and has a constant direction. $E_{\text{int}}(s, s-1)$ and $E_{\text{int}}(s, s+1)$ are the internal forces that simulates elastic force and formulate as follows:

$$E_{\text{int}}(s, s') = \text{sgn}(f(s') - f(s))\gamma^{|f(s')-f(s)|} \quad |f(s') - f(s)| < \phi \tag{12}$$

where $f(s)$ gives the coordinates of the control point s, and $\text{sgn}(f(s') - f(s))$ is the sign function that calculates the force direction. We constrain this force to be within the immediate neighbors. It is worth noting that the force direction depends on the relative location of the two points involved.

Fig. 4 illustrates snapshots of the evolution of a snake. At initialization, Fig. 4(a), control points are at the same altitude. An iteration is defined by moving all control points until balance is reached. In the next iteration, we reinitialize all the control points by increasing their location by one unit, as shown in Fig. 4(g). Control points are relocated into nontag region so that external forces take over the movement.

Erroneous indexing arises at inconsistent line length, e.g., when the top lines are shorter than the lines underneath and the snake lands on more than one tagline. To correct it, we verify the current index with the original label assigned by (11) and the primary index is given to the first group label seen by the snake. Other labels are considered inconsistent. Once the snake becomes stable, all the control points with inconsistent labels will be withdrawn by one unit. The correction is repeated for those points until their label becomes the primary index.

Due to quantization error, the total force on a control point could be nonzero and causes the control point moves back and forth infinitely. To address this issue, we gradually reduce the energy exponentially

$$E'(s) = E(s)(e^{-t} - 1) \tag{13}$$

where t denotes the time. Allowing enough time, the energy of a control point vanishes.

IV. Experiments and Evaluation

A. Image Acquisition and Preprocessing

In our studies, a 2-D slice was acquired with 1-D SPAMM [25] planar tagging for each task response. A modified real-time TrueFISP pulse sequence was used with parameters: 26× 20 cm field of view (FOV), 6 mm slice thickness, 60° flip angle, 256 frequency resolution, 50% phase resolution with 3/4 partial Fourier acquisition, 977 Hz per pixel bandwidth, 3.55 ms TR and 1.78 ms TE. The pixel size was 1.09375 mm × 1.09375 mm. We acquired three sets of images for every subject. Each set consists of nine images. We used images from six human subjects in our experiments. Before tagline detection, images were quantized to 8-bit grayscale and their histograms were stretched linearly to the 8-bit range.

B. Wavelet Decomposition Scale Analysis

In wavelet decomposition, the number of decomposition scales specifies the extent coarse features are analyzed. When a coarse scale is used, wide stripe features are extracted. This is analogous to using large filters used in the HARP method and Gabor-filter-based method. To study the impact of decomposition scale to tagline detection results, we applied our method to

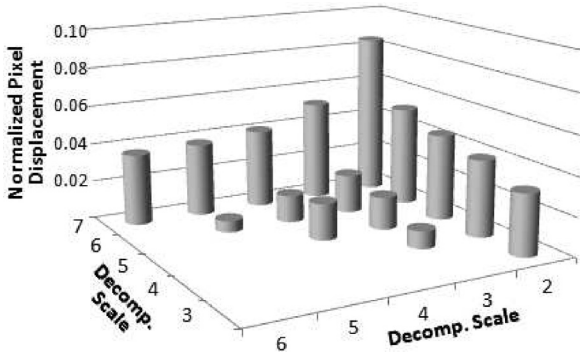

Fig. 5. Mean normalized pixel displacement with respect to decomposition scales.

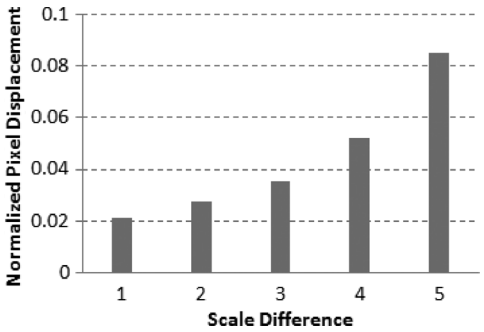

Fig. 6. Detection variance with respect to the scale differences.

20 randomly selected images and evaluated the tagline detected using decomposition scales 2 through 7.

We measured the consistency using a normalized pixel displacement $\mathcal{E}$, as follows:

$$\mathcal{E} = \frac{t_p \cup t_q - t_p \cap t_q}{t_p \cup t_q} \tag{14}$$

where $t_p \cup t_q$ is the union of two binary tagline images and $t_p \cap t_q$ is the intersection of these two images. The tagline pixels bear a value of 1; the background pixels bear a value of 0. Fig. 5 illustrates the average $\mathcal{E}$. The variation between two adjacent decomposition scales is mostly smaller when compared to that of the nonadjacent scales (The nonadjacent scale variations are plotted in Fig. 6.) However, the difference is minimal in general—less than 5% in the majority of cases. Hence, the variance induced by decomposition scale is negligible in our method.

Examples of tagline detected using different decomposition scales are illustrated in Fig. 7. It is shown that the detected taglines closely resemble one another. In the rest of our experiments, we used the decomposition scale of 4 in wavelet analysis.

C. Performance Evaluation

In performance evaluation, we randomly selected six sets of images and hand-traced the taglines. The hand-tracing results were cross validated by three individuals and then merged as reference. Due to the size of the human tongue, the number of taglines in each case differs. In our comparison study, we categorized taglines into two groups based on their curvature: slow changing taglines (SCT) and highly curving taglines (HCT).

Fig. 8 illustrates our results. There are seven to nine taglines in each image. The left panel in each example shows the original images and the right panel shows the detected taglines (in red) superimposed on the original images. Due to muscle contractions, some taglines depict an almost 90° deformation [see Fig. 8(a)].

To quantify tagline estimation errors, we calculated the pixel displacement $\mathcal{P}$ of the detected results against the reference taglines. Let l^r and l^t denote a reference tagline and a detected tagline, respectively. r_i and t_i are the corresponding pixels on each line. The tagline pixel displacement is the cumulative distance of all the corresponding pixels on l^r and l^t

$$\mathcal{P}(l^r, l^t) = \sum_{i=1}^{q} |t_i - r_i|. \tag{15}$$

For comparison, we implemented the HARP method [11]. We chose the filter size to be the distance between two adjacent spectrum peaks. The maximum gradient points in the reconstructed phase images were extracted and eroded with the same algorithm used in our method to reduce the tagline width to 1 pixel.

Table I shows the mean and the standard deviation (STD) of pixel displacement produced by our method and the HARP method. For slow changing taglines, both methods resulted in relative small errors. However, our algorithm demonstrated much less error when taglines exhibit larger curvature. In contrast, the mean error of the HARP method increased by 92% and STD increased by 79%, respectively. Using one-way ANOVA and means testing, we analyzed the performance of both methods. The results from both methods are balanced around their means (9.7 and 19.2 for our method and the HARP method, respectively). The means confidence interval is (5, 12) for our method and the confidence interval is (10, 25) for the HARP method. The confidence interval of our method is much smaller than that of the HARP method and there is little overlap between these confidence intervals. The p-value is 1E–6, which implies a significant improvement in accuracy and robustness.

Table II lists the pixel displacement for the images in Fig. 8. Taglines are numbered from top to bottom, and the taglines outside the human tongue region, showing no irrelevant tissue deformation, were not considered. By matching measurements in Table II with images, we can see that our method performed slightly better than the HARP method on average. However, the improvement becomes significant for highly curved lines and blurry lines. The HARP method resulted in $\mathcal{P} = 35$ for an almost 90° curved tagline [line 9 in Fig. 8(a)], whereas our method resulted in $\mathcal{P} = 11$. The blurry taglines also caused the HARP method to exhibit greater errors as shown in Fig. 8(c). For lines 7 and 8, our method resulted in $\mathcal{P} = 15$ and 9, respectively; whereas HARP resulted in $\mathcal{P} = 37$ and 52, respectively.

Fig. 9(a) and (d) illustrates the cropped tagged MR images in the region of tongue, which show taglines with great curvature and blurry taglines. Fig. 9(c) and (f) shows the results of the HARP method. Broken taglines are primarily due to the limit in

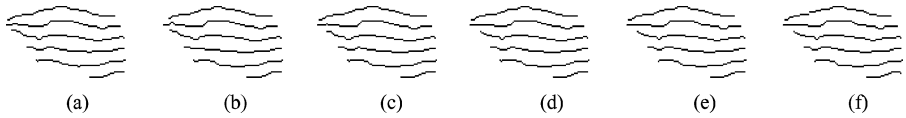

Fig. 7. Comparison of tagline detection using different wavelet decomposition scales. The numbers of scales used are 2–7 for (a)–(f), respectively.

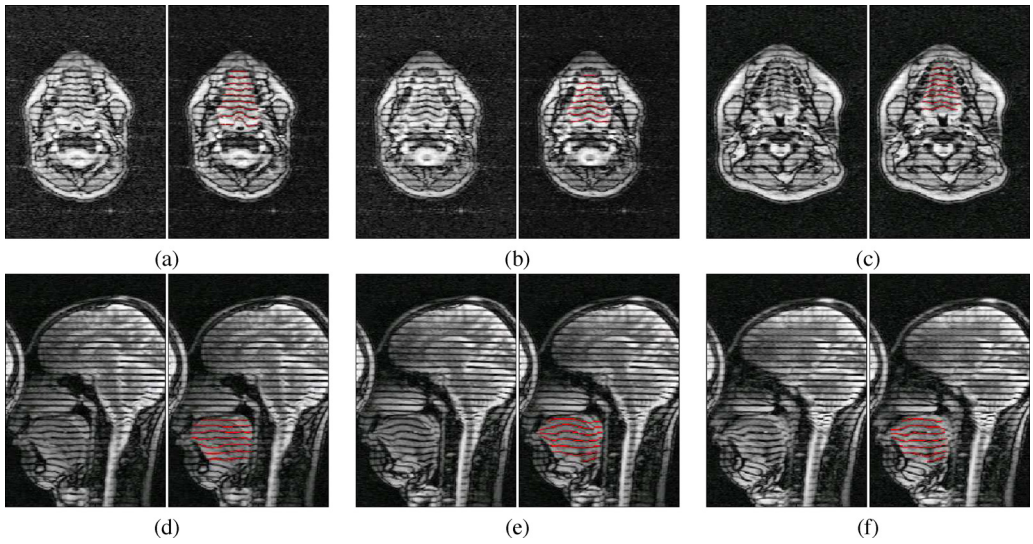

Fig. 8. Examples shows detected taglines superimposed on the original images. (a)–(c) Coronal images. (d)–(f) Sagittal images.

TABLE I
TAG PIXEL DISPLACEMENT MEASUREMENT

Methods	SCT		HCT	
	Mean	STD	Mean	STD
Our method	8.8	6.5	13.8	8
HARP method	11.2	5.8	26.5	10.4

TABLE II
TAG PIXEL DISPLACEMENT OF THE IMAGE SHOWN IN FIG. 8

Taglines	Img a	Img b	Img c	Img d	Img e	Img f
Our Method						
line 1	0	1	6	2	7	12
line 2	3	3	4	19	18	4
line 3	0	5	5	18	23	17
line 4	7	5	8	18	23	26
line 5	7	10	10	12	7	7
line 6	2	11	7	10	10	12
line 7	10	12	15	19	5	7
line 8	14	6	9			
line 9	11					
HARP Method						
line 1	9	8	8	11	18	25
line 2	6	4	14	18	16	36
line 3	10	5	10	29	22	26
line 4	9	12	19	19	36	20
line 5	8	16	13	38	20	29
line 6	23	17	17	28	15	36
line 7	20	21	37	11	10	6
line 8	22	19	52			
line 9	35					

spectral components recovered in the phase image after filtering. The erroneous tagline in Fig. 9(f) is very hard to correct because of the overlap. In practice, manual correction usually follows. The taglines illustrated in Fig. 9(b) and (e) are results of our method, which are very satisfactory.

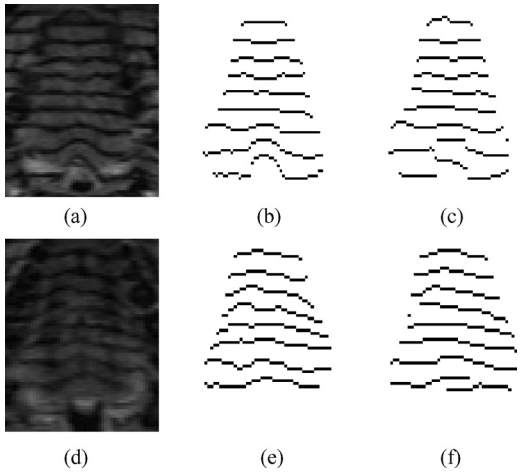

Fig. 9. Zoomed-in view of tagline results. (a) and (d) Original images. (b) and (e) Results of our method. (c) and (f) Results of the HARP method.

V. SUMMARY AND CONCLUSION

We have developed a novel multiresolution tagline detection and indexing method. The indexing step is an intrinsic process for tagline recovery. Our method is rooted in frequency analysis of the tMR images, and incorporates a snake method for tagline recovery and indexing.

Our method has been validated with 320 tMR tongue images from six human subjects. The results were compared with taglines detected using the HARP method and with manually traced references. The experiments demonstrated that our method produced taglines with greatly improved accuracy and robustness.

Further improvement includes an interpolation method that provides higher order smoothness, such as B-Splines. Also, time complexity of tagline detection algorithms will be explored in our future work. In our current studies, one or two human subjects are scanned in a week due to the limitations on subject selection, training, and scanner scheduling. However, algorithm efficiency shall be evaluated and better methods that balance efficiency and precision shall be identified to prepare for higher throughput image acquisition. Although, it has little impact on the accuracy of tagline detection, development of an automatic region-of-interest segmentation method will boost the usability of tagline detection and the tagged MR imaging.

ACKNOWLEDGMENT

The authors would like to thank Dr. G. Chi-Fishman and Dr. C. Ozturk for their advices and assistance in image acquisition.

REFERENCES

[1] L. Axel, A. Montillo, and D. Kim, "Tagged magnetic resonance imaging of the heart: a survey," *Med. Image Anal.*, vol. 9, pp. 376–393, 2005.

[2] Y. Chen and A. A. Amini, "A MAP framework for tag line detection in SPAMM data using markov random fields on the B-spline solid," *IEEE Trans. Med. Imag.*, vol. 21, no. 9, pp. 1110–1122, Sep. 2002.

[3] T. S. Denney, "Estimation and detection of myocardial tags in MR image without user-defined myocardial contours," *IEEE Trans. Med. Imag.*, vol. 18, no. 4, pp. 330–344, Apr. 1999.

[4] X. Deng and T. S. Denney, "Three-dimensional myocardial strain reconstruction from tagged MRI using a cylindrical B-spline model," *IEEE Trans. Med. Imag.*, vol. 23, no. 7, pp. 861–867, Jul. 2004.

[5] M. Kass, A. Witkin, and D. Terzopoulos, "Snakes: Active contour models," *Int. J. Comput. Vis.*, vol. 1, pp. 321–331, 1987.

[6] C. Xu and J. L. Prince, "Snakes, shapes, and gradient vector flow," *IEEE Trans. Image Process.*, vol. 7, no. 3, pp. 359–369, Mar. 1998.

[7] A. A. Young, D. L. Kraitchman, L. Dougherty, and L. Axel, "Tracking and finite element analysis of stripe deformation in magnetic resonance tagging," *IEEE Trans. Med. Imag.*, vol. 14, no. 3, pp. 413–421, Sep. 1995.

[8] P. Radeva, A. Amini, J. Huang, and E. Marti, "Deformable b-solids and implicit snakes for localization and tracking of MRI-spamm data," presented at the IEEE Workshop Math. Models Biomed. Image Anal., San Francisco, CA, Jun. 1996.

[9] A. A. Amini, Y. Chen, R. W. Curwen, V. Mani, and J. Sun, "Coupled B-snake grids and constrained thin-plate splines for analysis of 2-D tissue deformations from tagged MRI," *IEEE Trans. Med. Imag.*, vol. 17, no. 3, pp. 344–356, Jun. 1998.

[10] M. A. Guttman, E. A. Zerhouni, and E. R. McVeigh, "Fast, contourless tag segmentation and displacement estimation for analysis of myocardial motion," presented at the SMR/ESMRMB, Nice, France, Aug. 1995.

[11] N. F. Osman, E. R. McVeigh, and J. L. Prince, "Imaging heart motion using harmonic phase MRI," *IEEE Trans. Med. Imag.*, vol. 19, no. 3, pp. 186–202, Mar. 2000.

[12] N. F. Osman and J. L. Prince, "On the design of the bandpass filters in harmonic phase MRI," presented at the Int. Conf. Image Process., Vancouver, Canada, Sep. 2000.

[13] Z. Qian, A. Montillo, D. Metaxas, and L. Axel, "Segmenting cardiac MRI tagging lines using Gabor filter banks," in *Proc. 25th Int. Conf. IEEE EMBS*, Philadelphia, PA, Oct. 2003, pp. 630–633.

[14] Z. Qian, X. Huang, D. Metaxas, and L. Axel, "A robust segmentation of 4D cardiac MRI-tagged images via spatio-temporal propagation," in *Proc. SPIE Med. Imag.*, vol. 5746, 2005, pp. 580–591.

[15] S. Mallat and S. Zhong, "Characterization of signals from multiscale edges," *IEEE Trans. Pattern Anal. Mach. Intell.*, vol. 14, no. 7, pp. 710–732, Jul. 1992.

[16] R. C. Gonzalez and R. E. Woods, *Digital Image Processing*, 2nd ed. Englewood Cliffs, NJ: Prentice-Hall, 2002.

[17] A. Niedermeier, E. Romaneeben, and S. Lehner, "Detection of coastlines in SAR images using wavelet methods," *IEEE Trans. Geosci. Remote Sens.*, vol. 38, no. 5, pp. 2270–2281, Sep. 2000.

[18] P. Bao and L. Zhang, "Noise reduction for magnetic resonance images via adaptive multiscale products thresholding," *IEEE Trans. Med. Imag.*, vol. 22, no. 9, pp. 1089–1099, Sep. 2003.

[19] J. Liu and P. Moulin, "Information-theoretic analysis of interscale and intrascale dependencies between image wavelet coefficients," *IEEE Trans. Med. Imag.*, vol. 10, no. 11, pp. 1647–1658, Nov. 2001.

[20] L. Zhang, P. Bao, and X. Wu, "Hybrid inter- and intra-wavelet scale image restoration," *Pattern Recogn.*, vol. 36, pp. 1737–1746, 2003.

[21] N. Otsu, "A threshold selection method from gray-level histogram," *IEEE Trans. Syst. Man Cybern.*, vol. SMC-9, no. 1, pp. 62–66, Jan. 1979.

[22] V. Caselles, R. Kimmel, and G. Sapiro, "Geodesic active contours," *Int. J. Comput. Vis.*, vol. 22, no. 1, pp. 61–79, 1997.

[23] C. Sagiv, N. A. Sochen, and Y. Y. Zeevi, "Integrated active contour for texture segmentation," *IEEE Trans. Image Process.*, vol. 15, no. 6, pp. 1633–1646, Jun. 2006.

[24] Y. Xiang, A. C. Chung, and J. Ye, "An active contour model for image segmentation based on elastic interaction," *J. Comput. Phys.*, vol. 219, pp. 455–476, 2006.

[25] L. Axel and L. Dougherty, "MR imaging of motion with spatial modulation of magnetization," *Radiology*, vol. 171, pp. 841–845, 1989.

Xiaohui Yuan (M'05) received the B.S. degree in electrical engineering from Hefei University of Technology, Hefei, China, in 1996 and the Ph.D. degree in computer science from Tulane University, New Orleans, LA, in 2004.

He worked at the National Institutes of Health, MD on medical imaging and image analysis from 2005 to 2006 and joined the University of North Texas, Denton as an Assistant Professor in 2006. His research interests include computer vision, data mining, and artificial intelligence, and has been supported by NSF, Texas Advanced Research Program, and UNT.

Dr. Yuan is a member of Society of Photo-Optical Instrumentation Engineers (SPIE).

J. Zhang , photograph and biography not available at the time of publication.

B. P. Buckles , photograph and biography not available at the time of publication.